

Microwave-Assisted Synthesis, Microstructure and Magnetic Properties of Rare-Earth Cobaltites

Julia Gutiérrez Seijas¹, Jesús Prado-Gonjal¹, David Ávila¹, Ian Terry², Emilio Morán¹, Rainer Schmidt^{3,*}

¹*Dpto. Química Inorgánica I, Facultad CC. Químicas, Universidad Complutense de Madrid, 28040 Madrid, Spain.*

²*Dept. Physics, University of Durham, South Road, Durham DH1 3LE, United Kingdom.*

³*Dpto. Física Aplicada III, GFMC, Facultad CC. Físicas, Universidad Complutense de Madrid, 28040 Madrid, Spain.*

Abstract

The series of perovskite rare-earth (RE) doped cobaltites (RE)CoO₃ (RE = La – Dy) was prepared by microwave-assisted synthesis. The crystal structure undergoes a change of symmetry depending on the size of the RE cation. LaCoO₃ is rhombohedral, S.G. R-3c (No. 167), while for the rest of the RE series (Pr – Dy) the symmetry is orthorhombic, S.G. Pnma (No. 62). The crystal structure obtained by X-Ray diffraction was confirmed by high resolution transmission electron microscopy, which yielded a good match between experimental and simulated images. It is further shown that the well-known magnetism in LaCoO₃, which involves a thermally induced Co³⁺ (d⁶) low spin to intermediate or high spin state transition, is strongly modified by RE-doping and a rich variety of magnetic order has been detected across the series.

*Corresponding author. Email: rainerxschmidt@googlemail.com

1. Introduction

Perovskite rare-earth cobaltites (RE)CoO₃ have attracted considerable research interest recently due to their intriguing magnetic properties [1-3]. Additionally, useful material properties such as temperature-induced metal-insulator transitions and thermoelectricity have been reported as well [4-9]. In the work presented here we study microwave (MW) –assisted synthesis of the RE cobaltites (RE)CoO₃ (RE = La - Dy) series in order to demonstrate the feasibility of the MW technique for this class of materials. Furthermore, we show that the magnetism in microwave (MW) synthesized (RE)CoO₃ displays different types of magnetic ordering [8, 10], which depends on the RE cation and involves variation of the Co³⁺ spin state (electronic configuration: [Ar] 3d⁶). The Co³⁺ spin states may be (a) low-spin (LS) (t_{2g}⁶ e_g⁰), (b) intermediate-spin (IS) (t_{2g}⁵ e_g¹), or (c) high-spin (HS) (t_{2g}⁴ e_g²) [10-12]. The competition between different spin states has caused large controversy in the literature previously [10, 12-19], but in most studies only the case of LaCoO₃ has been considered. Different studies favor either a LS to IS or a LS to HS state transition by heating across $T_{s1} \approx 75$ K [20-24]. Furthermore, a low temperature magnetic defect structure has been commonly observed in LaCoO₃, which can be explained by the existence of magnetic polarons or excitons [24-27]. Here in this work we investigate the influence of the RE cation on the structural, microstructural and magnetic properties, in particular on the Co³⁺ spin-state, the spin-state transition and the magnetic defect structure.

RE-cobaltites are usually synthesized by solid-state reactions, where the process involves multiple heating (≥ 1200 °C) and regrinding steps to help overcome the solid-state diffusion barrier. Here we show that monophasic rare-earth cobaltite materials can be obtained by MW-assisted synthesis within 30 minutes with massive time and energy savings. LaCoO₃ has been synthesized previously by innovative and novel chemical synthesis methods [28-30], including MW-assisted processes [11, 31, 32], but the rest of the series (RE = Pr – Dy) has not been prepared before using MW heat sources to the best of our knowledge.

The crystal structure of the synthesized (RE)CoO₃ powders was investigated in detail by powder X-ray Diffraction (XRD) and High Resolution Transmission Electron Microscopy (HRTEM) to confirm the crystal structure type, symmetry and space group (S.G.). The microstructure and composition of our samples were determined by Field Emission Scanning Electron Microscopy (FE-SEM), Energy Dispersive Spectroscopy (EDS) of X-rays and Thermal Gravimetric Analysis (TGA). Furthermore, by using temperature dependent powder magnetometry we demonstrate that the spin-state, the spin-state transition, the effective magnetic moment μ_{eff} and the low temperature defect magnetism strongly vary across the (RE)CoO₃ (RE = Pr – Dy) series giving rise to a rich variety of magnetic ordering phenomena.

2. Experimental procedure

2.1 Synthesis

Appropriate amounts of precursor nitrates [98% Co(NO₃)₃·6H₂O and 99.9% (RE)(NO₃)₃·xH₂O, Sigma-Aldrich] were weighed and mixed with 5% (wt.%) amorphous carbon acting as a MW absorber due to its high electrical conductivity. The mixture was mechanically homogenized and compacted into pellets of 13 mm diameter, which were placed in a porcelain crucible and irradiated in a domestic microwave oven for 30 min (2.45 GHz and 800 W). The domestic microwave furnaces in our laboratories do not allow precise control of the reaction temperature [33, 34], but the pellets turned “red hot” after *ca.* 5 min of irradiation and the reaction completed rapidly within 30 min. Therefore, it seems certain that the reaction temperature would be well above 700 °C. The fast start-up of the heating process may at least partially be attributed to the presence of water of hydration in the precursor nitrates, where the polar H₂O molecules couple readily to the MWs [35]. Further possible contributions to the heating mechanism may arise from the formation of a highly conducting precursor cobalt oxide, and possibly the first (RE)CoO₃ clusters formed from the precursors. The cobaltite precursor, LaCoO₃ and possibly

all other (RE)CoO₃, can be expected to be electrically highly conducting at ambient and elevated temperatures. Therefore, they may act in a similar way as the black carbon added as a microwave absorber. It is unclear at this point to which extent each of these materials (nitrates, precursor cobaltite, (RE)CoO₃, black carbon) contribute to the overall heating process, but we can certainly confirm significant time and energy savings in the production of RE cobaltites (RE)CoO₃ using MW heat sources.

2.2 Structural and microstructural characterization

The phase purity of the obtained powders and ceramic pellets were tested by powder XRD using monochromatic Cu K α_1 radiation ($\lambda = 1.5406 \text{ \AA}$) on a Philips **X'Pert PRO ALPHA 1** high-resolution diffractometer. X-rays were detected with a solid-state X'Celetator RTMS detector. Structural Rietveld refinements from XRD patterns of all (RE)CoO₃ powders were carried out using FullProf software [36]. FE-SEM of gold-coated powders was carried out using a JEOL JSM 6400 microscope equipped with a detector for EDS of X-rays. Good homogeneity and the expected semiquantitative 1:1 cation compositions of RE/Co for all powders were confirmed. Samples for HRTEM were prepared from powders suspended and ultrasonically dispersed in butanol. One drop of the suspension was placed on a copper grid coated by a holey carbon film. Selected-area electron diffraction and HRTEM experiments were performed using a JEOL 3000F microscope with a resolution limit of $\approx 1.1 \text{ \AA}$. HRTEM images were recorded with an objective aperture of 70 μm centered on a sample spot within the diffraction pattern area. Fast Fourier Transforms (FFTs) of the HRTEM images were carried out to reveal the periodic image contents using the *Digital Micrograph* package [37]. The experimental HRTEM images were compared to simulated images using *MacTempas* software [38]. The relevant computations were performed using structural information from the Rietveld refinement procedure, the microscope parameters such as microscope operating voltage and spherical aberration, and the

specimen parameters such as zone axis and thickness. The defocus and sample thickness parameters were optimized by assessing the agreement between model and data.

Thermogravimetric analysis (TGA) was carried out to determine the oxygen content using a Cahn D-200 electrobalance on samples of about 50 mg in H₂ (200 mbar)/He (400 mbar) atmosphere upon heating up to 800 °C.

2.3 Magnetic property measurements

Magnetic susceptibility measurements of the synthesized powders were performed in a Quantum Design XL-SQUID magnetometer in the temperature range of 2 – 300 K using an applied magnetic field of $H = 10$ kOe. The temperature dependence of the magnetic susceptibility was measured following zero-field-cooled and field-cooled (ZFC-FC) procedures with intermediate demagnetization at room temperature.

3. Results and discussion

3.1 Composition and crystal structure

All microwave-synthesized (RE)CoO₃ powders (RE = La – Dy) were single phase, as confirmed by XRD. Figure 1 shows representative examples of XRD patterns and Rietveld refinement fits.

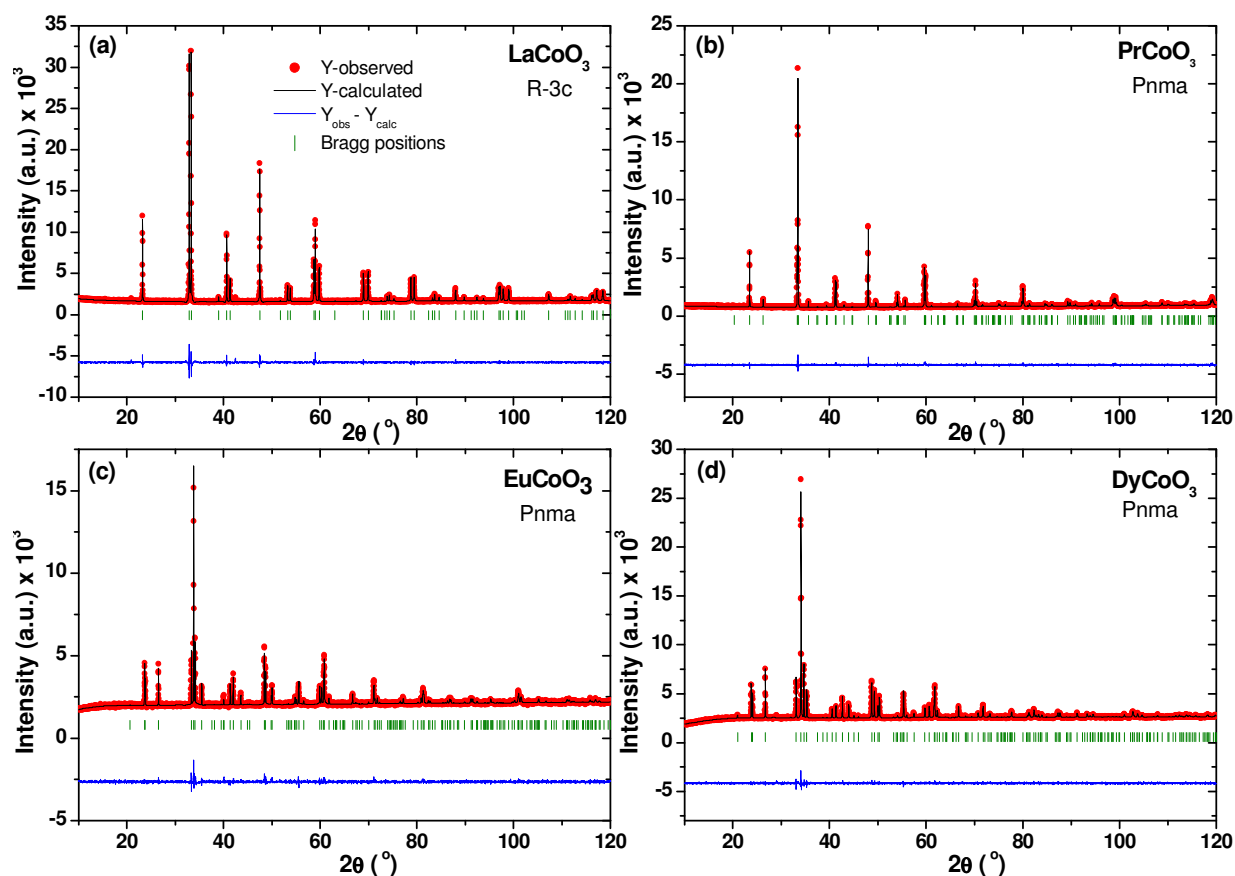


Figure 1. (a-d) Rietveld refinements of XRD patterns: observed (red dotted lines), refined (black solid lines) intensities, and their difference (blue bottom line). Green or blue vertical bars indicate the reference reflection positions.

The parameters obtained from the structural refinements are presented in the Supporting Information (Tables 1 a,b,c) including lattice parameters, atomic positions, tilting angles and bonding distances.

For smaller RE cations (RE = Ho – Lu) the perovskite phase cannot be crystallized by microwave irradiation. A mixture of RE and cobalt oxides was identified in this case by XRD. The smaller RE cations lead to a too high degree of octahedral distortions and no single phase perovskite structure can be observed for RE = Ho – Lu. This is somewhat surprising though, because the perovskite tolerance factor t would still be within the reported stability limits of $t = 0.8 - 1$ for a perovskite phase to form. The instability of the perovskite phase for (RE = Ho –

Lu) may be related to the difficulty to stabilize Co^{3+} and increasingly oxidizing conditions would be required. These perovskite phases can be stabilized though by high pressure synthesis (2 GPa at 900 °C for 25 minutes)[39].

For our MW-synthesized samples a change of symmetry occurs from rhombohedral in LaCoO_3 , S.G. R-3c (no. 167), to orthorhombic for the rest of the series (RE = Pr – Dy), S.G. Pnma (No. 62). The cell parameters a , b , and c for the RE family (RE = Pr – Dy) are given in Figure 2 as function of the RE ionic radius (IOR) and the tolerance factor t . IOR values were taken from Shannon's tables [40], where the coordination number 9 was considered for all RE cations consistently.

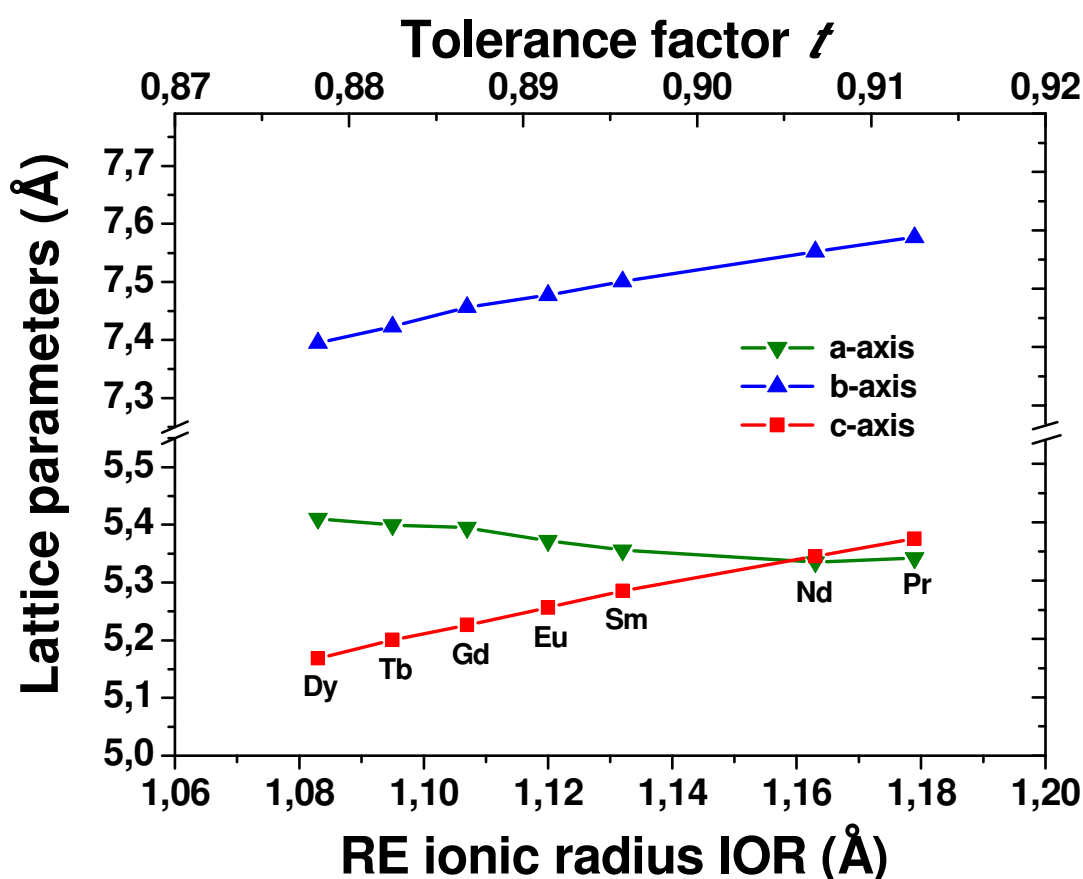


Figure 2. Lattice parameters a , b and c versus the RE IOR and the perovskite tolerance factor for the (RE) CoO_3 series. An approximately linear increase of b and c with IOR implies an increasing unit cell size.

Figure 2 shows approximately constant unit cell parameters a , whereas b and c decrease with decreasing IOR as a result of the decreasing unit cell size. The octahedral tilting angles θ , φ , μ (see Supporting Information Table 1c) all increase with decreasing IOR. This is consistent with the isostructural perovskite $Pnma$ (RE)CrO₃ series (RE = La – Lu), where the equivalent trends of cell parameters a , b , c and tilting angles θ , φ , μ with the IOR of the RE cation had been observed [34]. The rigid CoO₆ and CrO₆ octahedra both accommodate A-site RE cations of decreasing size by decreasing the unit cell size and increasing the degree of octahedral tilting.

3.2 Microstructural characterization

3.2.1 FE-SEM

Figure 3 shows two representative FE-SEM micrographs for (a) SmCoO₃ and (b) GdCoO₃ powders. A uniform morphology with considerable porosity and the formation of larger agglomerates of smaller particles can be observed. The remaining powders all show the equivalent features. These findings are quite different to the observations made previously across the isostructural (RE)CrO₃ series, where considerable variation in the particle shape, morphology and agglomeration had been observed [34].

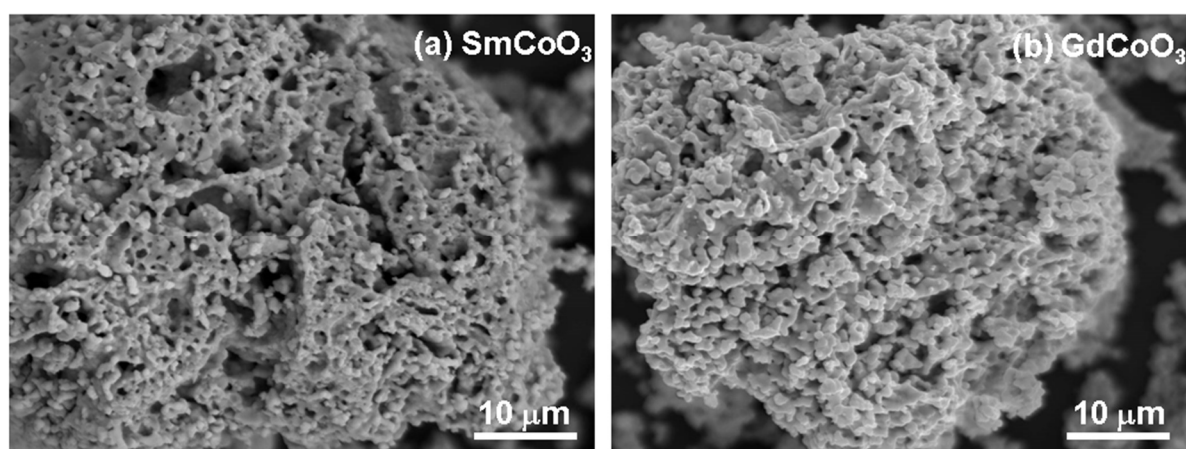


Figure 3. FE-SEM micrographs of powder samples of (a) SmCoO₃, and (b) GdCoO₃.

This indicates that the (RE)CoO₃ series may be less prone to microstructural changes due to a different B-site cation. This is an important finding, because MW-assisted synthesis is often associated with unfavorable and uncontrollable changes in particle microstructure, which is not the case here.

3.2.2. HRTEM

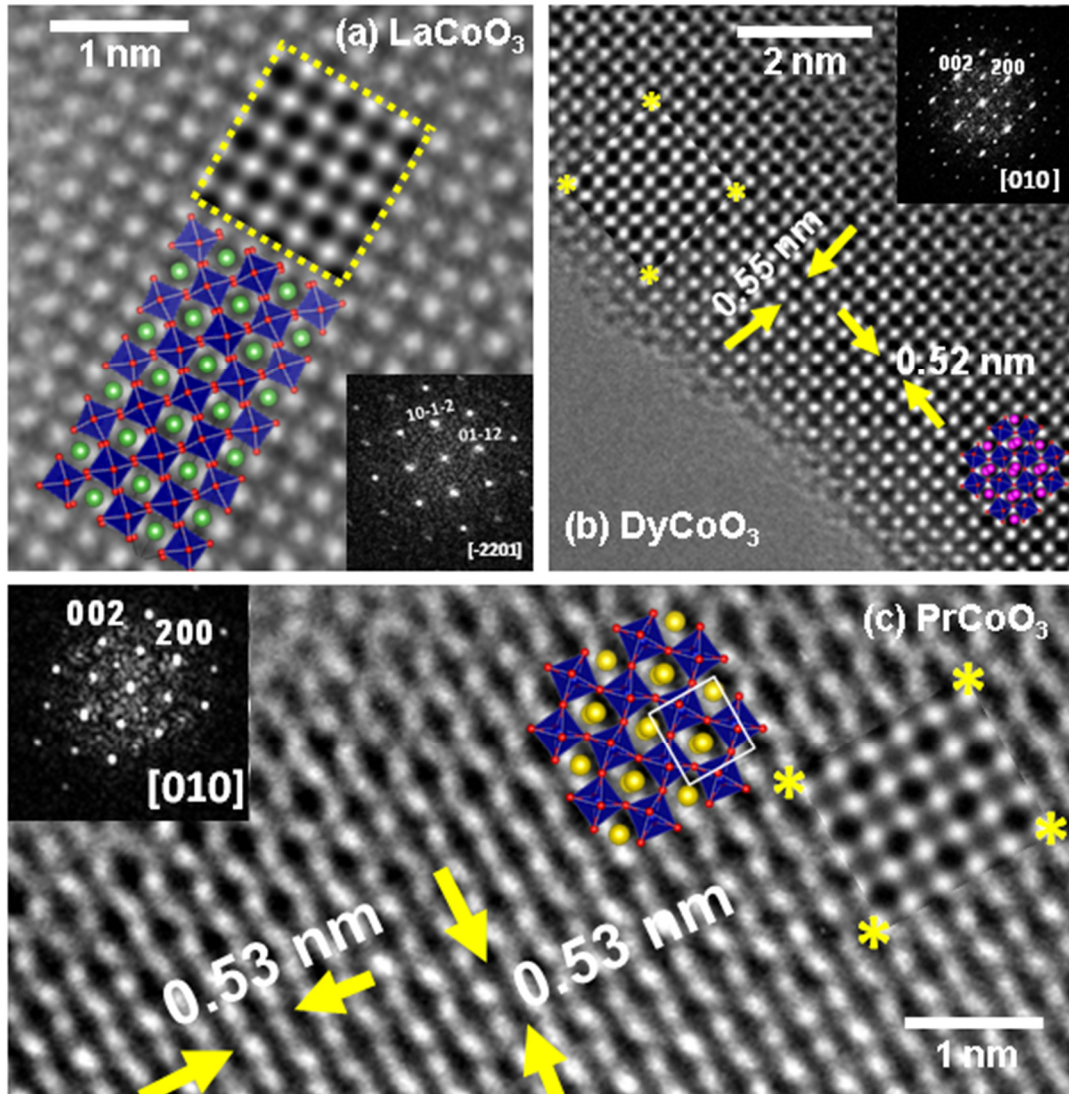


Figure 4. Experimental HRTEM micrographs along the [-2201] and [010] zone axis for (a) R-3c LaCoO₃, and Pnma (b) DyCoO₃ and (c) PrCoO₃. No streaking or extra spots are evident (see the FFT images in the figure insets). A good match between experimental and simulated images (rectangles marked by yellow dots or asterisks) is demonstrated.

HRTEM images for (RE)CoO₃ (RE = La, Pr, and Dy) are displayed in Figure 4. The experimental images taken along the [-2201] zone axis for LaCoO₃, and [010] for PrCoO₃ and DyCoO₃ show excellent agreement with the simulated images, which are depicted within the rectangles marked with (yellow) dots or asterisks. In all images, the black dots are the projections of the atomic columns from the RE and cobalt cation sublattices, showing a well-ordered crystal without the formation of superstructures or defects such as dislocations and stacking faults. This is evidenced by a regular contrast across the HRTEM images and the absence of extra spots or streaking lines in the FFTs (Figure 4 insets).

3.3 Oxygen content

The oxygen contents of all samples have been determined by TGA in hydrogen atmosphere. Thermogravimetric reduction curves of the LaCoO₃ and PrCoO₃ are presented in Figure 5. Two steps in the decomposition processes are apparent and approximately ideal stoichiometry was found for both initial compounds. In previous work it has been reported that oxygen vacancies commonly occur in LaCoO_{3-δ} [41] <Ref> and also in the rest of the (RE)CoO₃ (RE = Pr – Dy) series [42], where the vacancies are compensated by the formation of Co²⁺ cations. These Co²⁺ cations constitute magnetic impurities, which have been shown recently to act as nucleation centers for the formation of higher spin states across the spin-state transition [11].

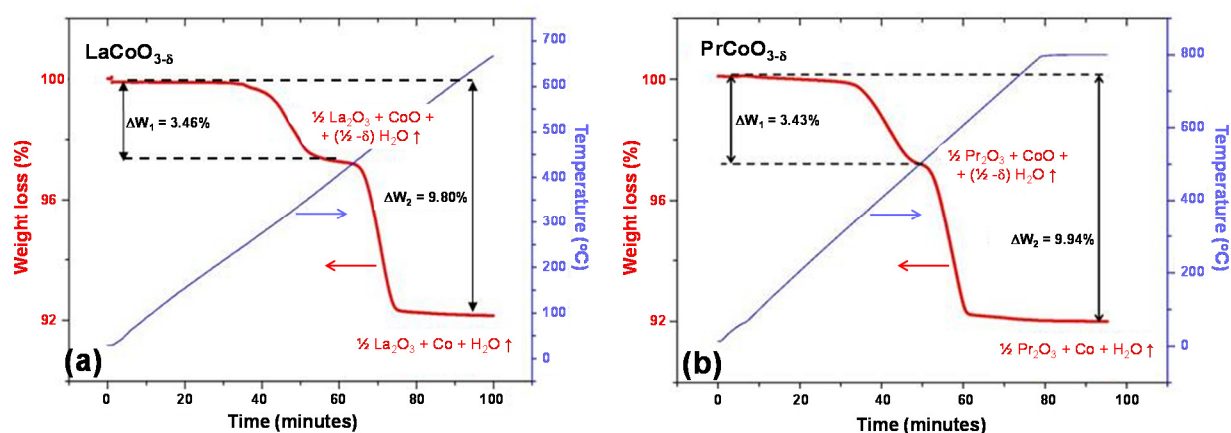


Figure 5. TGA curves corresponding to the H₂/He reduction of (a) LaCoO₃ and (b) PrCoO₃.

However, the weight loss measured here indicated that possible oxygen vacancies in all synthesized powder samples would exhibit a small concentration below the resolution limit of the TGA balance.

3.4 Magnetic properties

The susceptibility χ versus temperature T curves recorded at 10 kOe for powder samples of all (RE)CoO₃ (RE = La – Dy) compositions are shown in Figure 6. For all samples investigated no significant differences between the ZFC and FC curves occur and only the ZFC curves are shown in Figure 6. This is a fundamental difference as compared to the isostructural (RE)CrO₃ (RE = La – Lu) series, where significant and rather unusual variations between ZFC and FC curves had been observed [34].

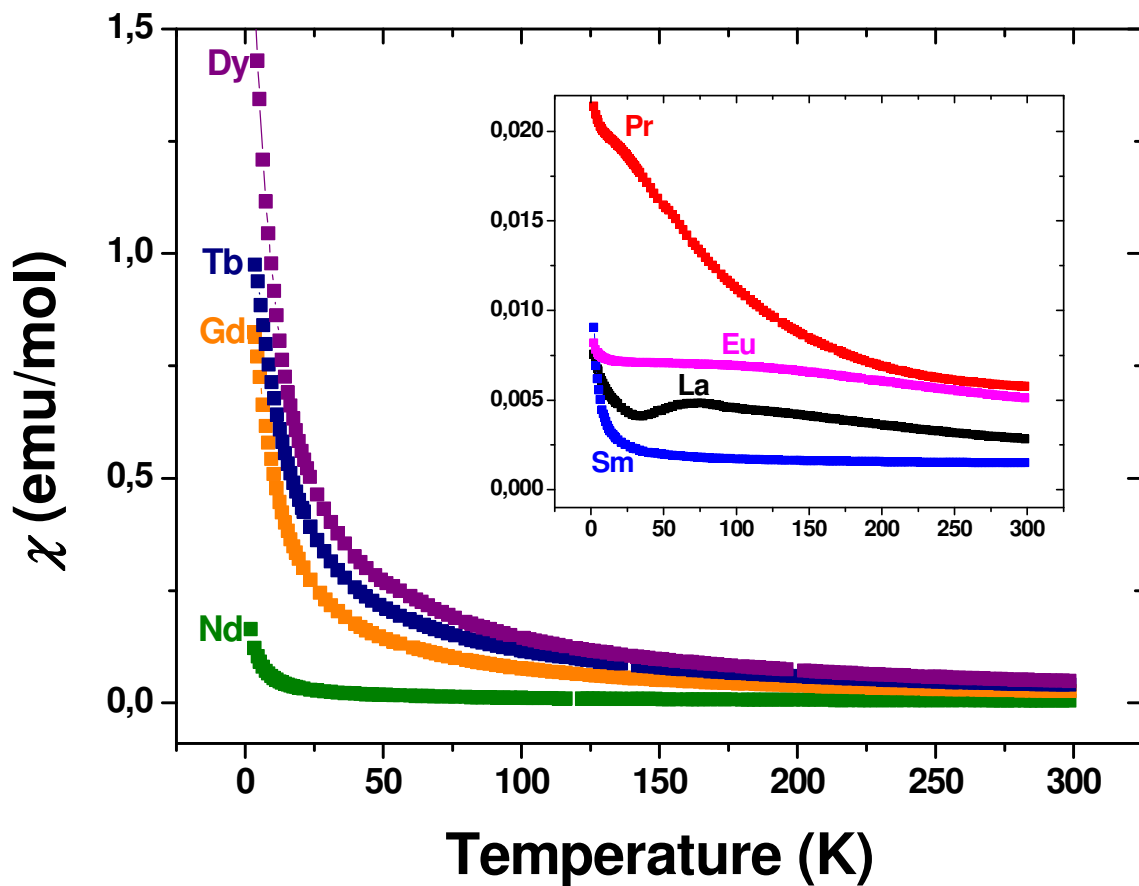


Figure 6. ZFC mass magnetic susceptibility χ versus temperature T measured in an applied magnetic field of $H = 10$ kOe for (RE)CoO₃ (RE = La – Dy).

These ZFC/FC variations in the (RE)CrO₃ series [34] may therefore be attributed to the effect of the Cr³⁺ magnetism and possibly its interaction with the RE magnetic moments, whereas the Co³⁺ magnetic moments appear to give rise to a more conventional magnetic behavior.

The Figure 6 inset shows the magnified χ vs T curves for La, Pr, Sm and Eu cobaltites, which all possess a significantly lower magnetization as compared to the rest of the series. The typical spin-state transition in LaCoO₃ in form of a peak in χ versus T at ≈ 75 K is displayed, whereas the transition in PrCoO₃ at ≈ 30 K may be less clearly developed. The magnified image in Figure 7 shows the spin-state transition of LaCoO₃ in more detail and the EuCoO₃ may in fact display a transition as well in form of a very broad peak around 110 K.

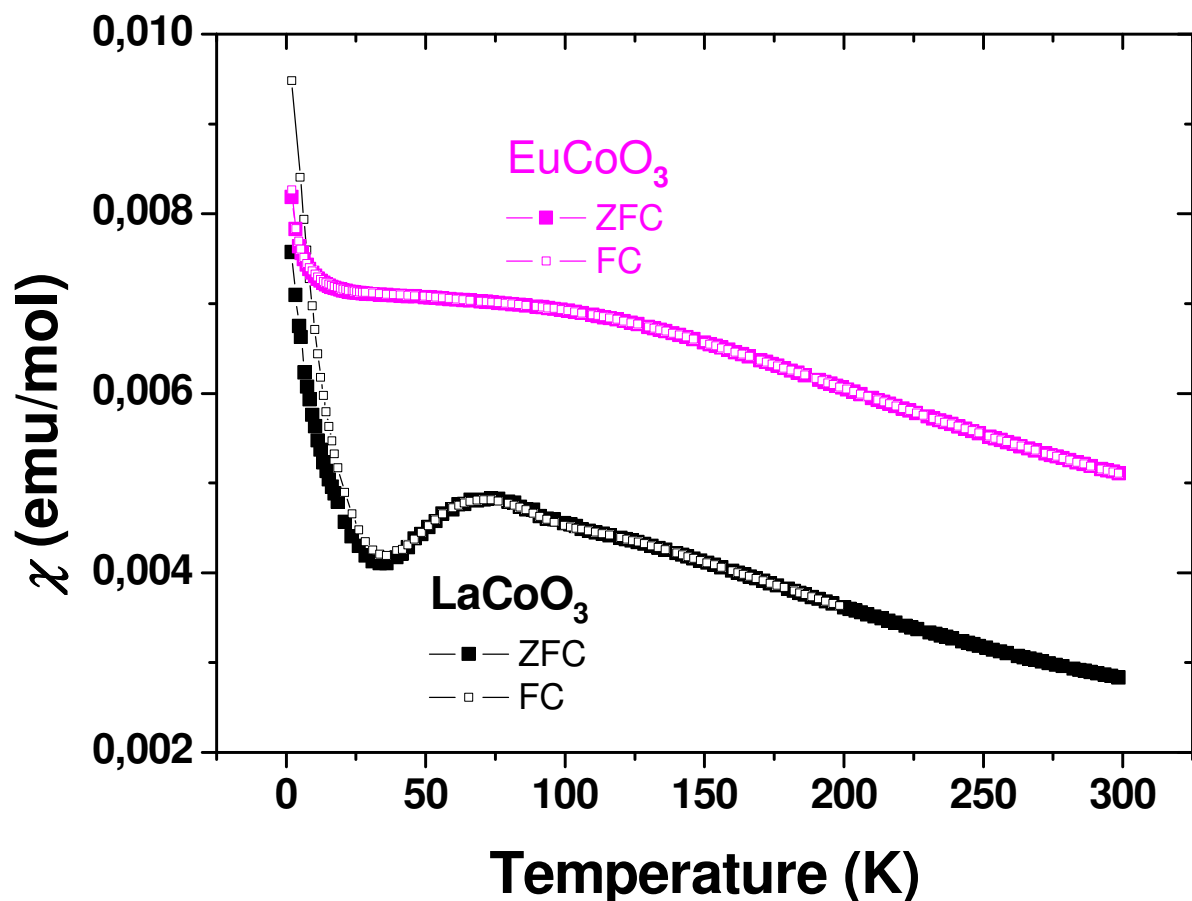


Figure 7. ZFC and FC (1 kOe) mass magnetic susceptibility χ versus temperature T for (RE)CoO₃ (RE = La, Eu).

However, only the χ vs T curves for LaCoO_3 , PrCoO_3 and EuCoO_3 show certain signs of a spin-state transition, whereas the curves for all other compositions do not show transitional features. This will be discussed in more detail below.

Figure 7 further demonstrates the differences between the ZFC and FC curves in detail, which are relatively small in EuCoO_3 whereas all other samples show negligible differences. Only in LaCoO_3 more perceptible deviations between ZFC and FC can be seen at low T where the defect magnetism is active. This is in agreement with previous work on conventionally synthesized LaCoO_3 [2].

All χ vs T curves presented in Figure 6 & 7 show the typical upturn in χ upon cooling to low T in form of a Curie-tail, which can be interpreted as a reflection of the ordering of magnetic defects such as the Co^{2+} cations that form due to oxygen vacancies [26, 43]. Although it may be difficult to precisely quantify the oxygen vacancy concentration from the Curie-tail, the rather small tail in EuCoO_3 may well be associated with a smaller amount of magnetic defects, whereas the larger tail in other compositions may be attributed to larger concentrations of defects and oxygen vacancies.

In the strictly paramagnetic state above the possible spin-state transitions the data from all samples follow the Curie-Weiss law: $\chi = C/(T - \theta)$, where C is the Curie constant related to the effective magnetic moment μ_{eff} and θ is the Weiss constant. Figure 8 shows the temperature dependence of the reciprocal magnetic susceptibility $1/\chi$, where the Curie-Weiss fits are indicated by red solid lines. In the Supporting Information the fitted C and θ , and the resulting μ_{eff} values are summarized. The θ values obtained from the fits are all negative, which indicates predominantly antiferromagnetic exchange interactions. Additionally, the theoretical values for μ_{eff} have been calculated for 3 potential cases by assuming that the Co^{3+} cation may be in the HS, IS or LS state.

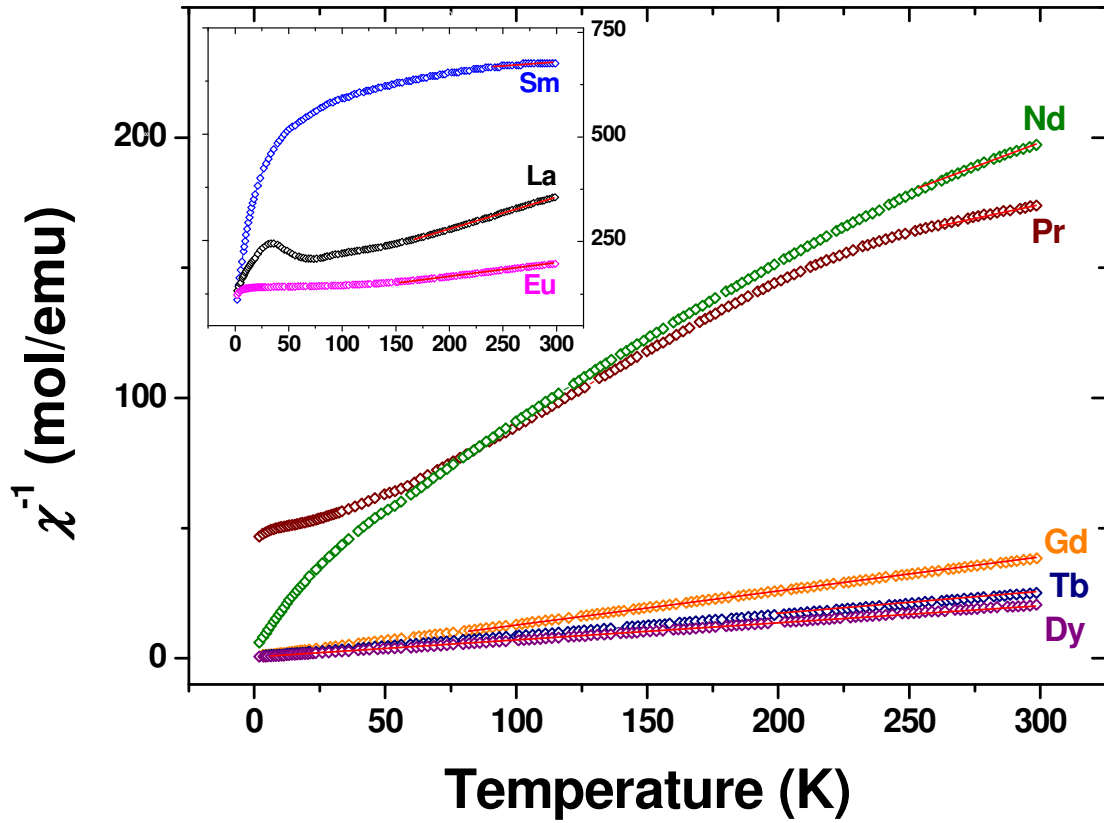


Figure 8. Inverse magnetic susceptibility $1/\chi$ versus T . Solid lines indicate the Curie-Weiss fits for determining the effective magnetic susceptibility μ_{eff} .

The experimental (black curve) and theoretical values for μ_{eff} are compared in Figure 9, where the theoretical values are represented by the green, blue and red curves for the Co^{3+} LS, IS and HS states respectively. Figure 9 indicates that the La, Pr and Sm containing cobaltites may be in a mixed spin state somewhere in between the IS and HS states at elevated temperatures where the Curie-Weiss law was applied. This is consistent with the literature in the case of LaCoO_3 . In fact, this mixed behavior may be regarded as the key issue regarding the large controversy in the literature on whether IS or HS state models are more suitable to describe the magnetism of the Co^{3+} cation above T_{s1} in LaCoO_3 . The existence of intermediate IS/HS states at higher T in La and Pr cobaltites may be consistent with the fact that both materials display the features of spin state transitions from an LS to a higher state (most likely mixed IS/HS) at ≈ 75 K and ≈ 30 K respectively.

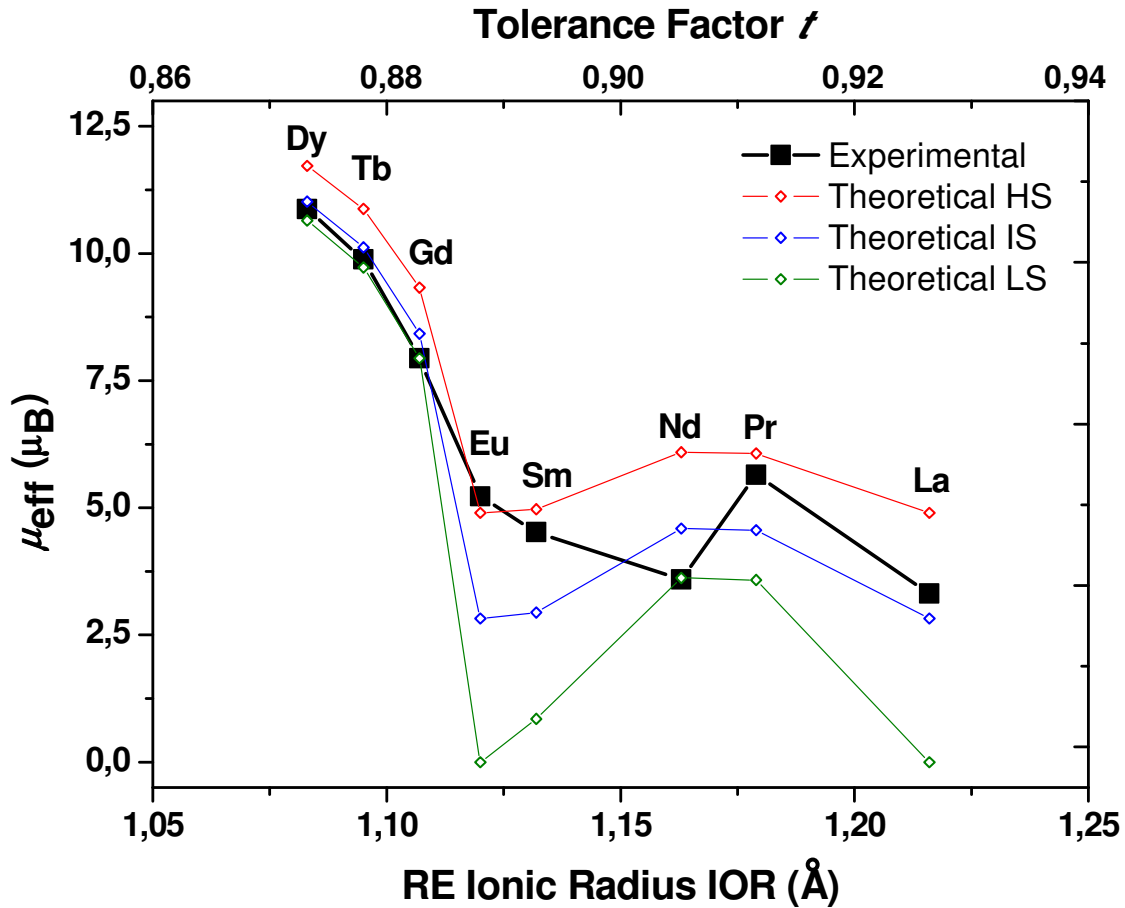


Figure 9. Effective magnetization μ_{eff} for (RE)CoO₃ (RE = Pr – Dy) obtained from the Curie-Weiss fits (■) and theoretical values for Co³⁺ high spin HS (red), intermediate spin IS (blue) and low spin LS (green) electron configurations.

On the other hand, the Eu cobaltite is found to be in a HS state above the spin state transition around 110 K, which may correspond to a broad LS to HS state transition (see also Figure 7). For the data at higher T , where the Curie-Weiss fits were obtained, the Nd, Gd, Tb and Dy cobaltites are found to be most likely in a LS state (Figure 9), which is consistent with the absence of any signs for spin-state transitions at all temperatures investigated (Figure 6). Furthermore, the Sm cobaltite is found to be in a mixed IS/HS state similar to the Pr sample, although no clear spin-state transition is displayed in Figure 6. However, Figure 8 shows some rather weak signs of transitional features at ≈ 60 K, which could be an indication for a LS to

IS/HS spin-state transition that is overlaid by a relatively large magnetic Curie-tail. This Curie-tail can again be interpreted as an indication for a certain magnetic defect concentration. Generally, no clear trend can be observed in Figure 9 between the spin-state obtained from Curie-Weiss fits and the size of the RE cation in terms of the IOR. It may therefore be concluded that the Co^{3+} spin-state may largely depend on other factors rather than the size of the RE cation, for example on the size of the RE magnetic moments and their interaction with the Co^{3+} magnetism, or interactions with the magnetic defect structure including Co^{2+} . In summary, LaCoO_3 , PrCoO_3 and SmCoO_3 show signs of LS to mixed IS/HS transitions of the Co^{3+} cation at ≈ 75 K, 30 K and 60 K respectively, whereas EuCoO_3 may exhibit a broad LS to HS transition around 110 K. NdCoO_3 , GdCoO_3 , TbCoO_3 and DyCoO_3 may adapt LS states consistently up to room temperature without the signs of spin-state transitions.

4. Conclusions

The perovskite series $(\text{RE})\text{CoO}_3$ ($\text{RE} = \text{La} - \text{Dy}$) was successfully prepared by a fast and simple microwave synthesis route for the first time using a domestic microwave oven. A structural change from R-3c to Pnma perovskite symmetry occurs between LaCoO_3 and PrCoO_3 . The unit cell parameters b and c , the perovskite tilting angles θ , φ and μ , and the spin states, spin-state transitions and μ_{eff} values strongly vary across the $(\text{RE})\text{CoO}_3$ series ($\text{Re} = \text{Pr} - \text{Dy}$).

Acknowledgments

E.M and J.P.G. are grateful to the Comunidad Autónoma de Madrid for providing financial support (Materyener3 S2013/MIT-2753 project). The authors wish to thank Dr. Julio Romero (CAI Técnica Físicas UCM) for carrying out magnetization measurements.

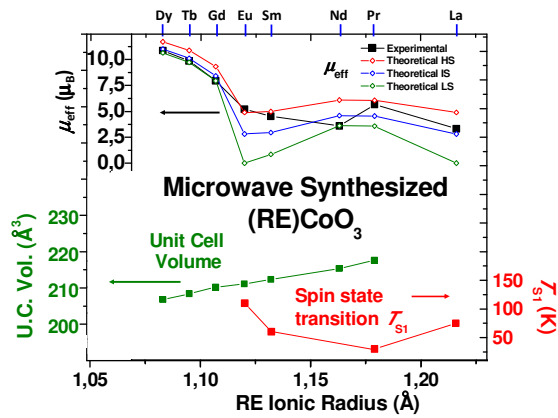
References

1. Deac, I. G.; Tetean, R.; Balasz, I.; Burzo, E., Low-temperature magnetic ordering in the perovskites $\text{Pr}_{1-x}\text{A}_x\text{CoO}_3$ (A=Ca, Sr). *Journal of Magnetism and Magnetic Materials* **2010**, 322, (9–12), 1185-1188.
2. Schmidt, R.; Wu, J.; Leighton, C.; Terry, I., Dielectric response to the low-temperature magnetic defect structure and spin state transition in polycrystalline LaCoO_3 . *Phys. Rev. B* **2009**, 79, 125105.
3. Troyanchuk, I. O.; Bushinskii, M. V.; Karpinsky, D. V.; Dobryanskii, V. M.; Sikolenko, V. V.; Balagurov, A. M., Positive magnetoresistance effect in rare earth cobaltites. *JETP Letters* **2009**, 89, (7), 319-323.
4. Nekrasov, I. A.; Streltsov, S. V.; Korotin, M. A.; Anisimov, V. I., Influence of rare-earth ion radii on the low-spin to intermediate-spin state transition in lanthanide cobaltite perovskites: LaCoO_3 versus HoCoO_3 . *Physical Review B* **2003**, 68, (23), 235113.
5. García-Muñoz, J. L.; Frontera, C.; Barón-González, A. J.; Valencia, S.; Blasco, J.; Feyerherm, R.; Dudzik, E.; Abrudan, R.; Radu, F., Valence transition in (Pr, Ca) CoO_3 cobaltites: Charge migration at the metal-insulator transition. *Physical Review B* **2011**, 84, (4), 045104.
6. Mineshige, A.; Inaba, M.; Yao, T.; Ogumi, Z.; Kikuchi, K.; Kawase, M., Crystal Structure and Metal–Insulator Transition of $\text{La}_{1-x}\text{Sr}_x\text{CoO}_3$. *Journal of Solid State Chemistry* **1996**, 121, (2), 423-429.
7. Maignan, A.; Hébert, S.; Pi, L.; Pelloquin, D.; Martin, C.; Michel, C.; Hervieu, M.; Raveau, B., Perovskite manganites and layered cobaltites: potential materials for thermoelectric applications. *Crystal Engineering* **2002**, 5, (3), 365-382.
8. Maignan, A.; Motohashi, T.; Hébert, S.; Pelloquin, D.; Raveau, B., Cobaltites: New materials with magnetoresistance properties. *Materials Science and Engineering: B* **2006**, 126, (2–3), 296-299.
9. Wang, Y.; Li, F.; Xu, L.; Sui, Y.; Wang, X.; Su, W.; Liu, X., Large Thermal Conductivity Reduction Induced by La/O Vacancies in the Thermoelectric LaCoO_3 System. *Inorganic Chemistry* **2011**, 50, (10), 4412-4416.
10. Korotin, M. A.; Ezhov, S. Y.; Solovyev, I. V.; Anisimov, V. I.; Khomskii, D. I.; Sawatzky, G. A., Intermediate-spin state and properties of LaCoO_3 . *Phys. Rev. B* **1996**, 54, (8), 5309.
11. Prado-Gonjal, J.; Gutiérrez-Seijas, J.; Anzorregui, I. H.; Morán, E.; Terry, I.; Schmidt, R., The role of defects in microwave and conventionally synthesized LaCoO_3 perovskite. *Journal of the European Ceramic Society* **2016**, 36, (5), 1197-1206.
12. Jonker, G., Magnetic and Semiconducting Properties of Perovskites Containing Manganese and Cobalt. *Journal of Applied Physics* **1966**, 37, (3), 1424-1430.
13. Louca, D.; Sarrao, J. L., Dynamical Disorder of Spin-Induced Jahn-Teller Orbitals with the Insulator-Metal Transition in Cobaltites. *Physical Review Letters* **2003**, 91, (15), 155501.
14. Ishikawa, A.; Nohara, J.; Sugai, S., Raman Study of the Orbital-Phonon Coupling in LaCoO_3 . *Physical Review Letters* **2004**, 93, (13), 136401.
15. Heikes, R. R.; Miller, R. C.; Mazelsky, R., Magnetic and electrical anomalies in LaCoO_3 . *Physica* **1964**, 30, (8), 1600-1608.
16. Raccah, P. M.; Goodenough, J. B., First-Order Localized-Electron - Collective-Electron Transition in LaCoO_3 . *Physical Review* **1967**, 155, (3), 932.
17. Haverkort, M. W.; Hu, Z.; Cezar, J. C.; Burnus, T.; Hartmann, H.; Reuther, M.; Zobel, C.; Lorenz, T.; Tanaka, A.; Brookes, N. B.; Hsieh, H. H.; Lin, H. J.; Chen, C. T.; Tjeng, L. H., Spin State Transition in LaCoO_3 Studied Using Soft X-ray Absorption Spectroscopy and Magnetic Circular Dichroism. *Phys. Rev. Lett.* **2006**, 97, (17), 176405.
18. Podlesnyak, A.; Streule, S.; Mesot, J.; Medarde, M.; Pomjakushina, E.; Conder, K.; Tanaka, A.; Haverkort, M. W.; Khomskii, D. I., Spin-State Transition in LaCoO_3 : Direct Neutron Spectroscopic Evidence of Excited Magnetic States. *Physical Review Letters* **2006**, 97, (24), 247208.

19. Zobel, C.; Kriener, M.; Bruns, D.; Baier, J.; Grüninger, M.; Lorenz, T.; Reutler, P.; Revcolevschi, A., Evidence for a low-spin to intermediate-spin state transition in LaCoO₃. *Phys. Rev. B* **2002**, 66, (2), 020402.
20. Imada, M.; Fujimori, A.; Tokura, Y., Metal-insulator transitions. *Rev. Mod. Phys.* **1998**, 70, (4), 1039.
21. Asai, K.; Gehring, P.; Chou, H.; Shirane, G., Temperature-induced magnetism in LaCoO₃. *Phys. Rev. B* **1989**, 40, (16), 10982.
22. Vogt, T.; Hriljac, J. A.; Hyatt, N. C.; Woodward, P., Pressure-induced intermediate-to-low spin state transition in LaCoO₃. *Phys. Rev. B* **2003**, 67, (14), 140401.
23. Burley, J. C.; Mitchell, J. F.; Short, S., Competing electronic ground states in La_{1-x}Ca_xCoO₃. *Phys. Rev. B* **2004**, 69, (5), 054401.
24. Yamaguchi, S.; Okimoto, Y.; Taniguchi, H.; Tokura, Y., Spin-state transition and high-spin polarons in LaCoO₃. *Phys. Rev. B* **1996**, 53, R2926.
25. Podlesnyak, A.; Russina, M.; Furrer, A.; Alfonsov, A.; Vavilova, E.; Kataev, V.; Büchner, B.; Strässle, T.; Pomjakushina, E.; Conder, K., Spin-state polarons in lightly-hole-doped LaCoO₃. *Physical Review Letters* **2008**, 101, (24), 247603.
26. Giblin, S. R.; Terry, I.; Clark, S. J.; Prokscha, T.; Prabhakaran, D.; Boothroyd, A. T.; Wu, J.; Leighton, C., Observation of magnetic excitons in LaCoO₃. *Europhys. Lett.* **2005**, 70, (5), 677-683.
27. Giblin, S. R.; Terry, I.; Prabhakaran, D.; Boothroyd, A. T.; Leighton, C., Low-temperature interactions of magnetic excitons in LaCoO₃. *Physical Review B* **2009**, 79, (17), 174410.
28. Liu, Y.; Dai, H.; Deng, J.; Zhang, L.; Zhao, Z.; Li, X.; Wang, Y.; Xie, S.; Yang, H.; Guo, G., Controlled Generation of Uniform Spherical LaMnO₃, LaCoO₃, Mn₂O₃, and Co₃O₄ Nanoparticles and Their High Catalytic Performance for Carbon Monoxide and Toluene Oxidation. *Inorganic Chemistry* **2013**, 52, (15), 8665-8676.
29. Predoana, L.; Malic, B.; Kosec, M.; Carata, M.; Calderaru, M.; Zaharescu, M., Characterization of LaCoO₃ powders obtained by water-based sol-gel method with citric acid. *Journal of the European Ceramic Society* **2007**, 27, (13-15), 4407-4411.
30. Popa, M.; Calderon-Moreno, J. M., Lanthanum cobaltite nanoparticles using the polymeric precursor method. *Journal of the European Ceramic Society* **2009**, 29, (11), 2281-2287.
31. Jung, W. Y.; Hong, S.-S., Synthesis of LaCoO₃ nanoparticles by microwave process and their photocatalytic activity under visible light irradiation. *Journal of Industrial and Engineering Chemistry* **2013**, 19, (1), 157-160.
32. Malghe, Y. S.; Gurjar, A. V.; Dharwadkar, S. R., Synthesis of LaCoO₃ from lanthanum trisoxalatocobaltate(III) (LTC) precursor employing microwave heating technique. *Journal of Thermal Analysis and Calorimetry* **2004**, 78, (3), 739-744.
33. Prado-Gonjal, J.; Schmidt, R.; Ávila, D.; Amador, U.; Morán, E., Structural and physical properties of microwave synthesized orthorhombic perovskite erbium chromite ErCrO₃. *Journal of the European Ceramic Society* **2012**, 32, (3), 611-618.
34. Prado-Gonjal, J.; Schmidt, R.; Romero, J.-J.; Avila, D.; Amador, U.; Moran, E., Microwave-Assisted Synthesis, Microstructure, and Physical Properties of Rare-Earth Chromites. *Inorganic Chemistry* **2013**, 52, 313-320.
35. Schmidt, R.; Prado-Gonjal, J.; Moran, E., Microwave-assisted hydrothermal synthesis of nanoparticles. In *CRC Concise Encyclopedia of Nanotechnology*, Kharisov, B.; Kharissova, O.; Ortiz-Mendez, U., Eds. CRC Press Taylor & Francis Group: Boca Raton (USA), 2015.
36. Rodriguez-Carvajal, J., A program for Rietveld refinement and pattern matching analysis. *Satellite Meeting of the XVth Congress of the Int. Union of Cryst. Toulouse* **1990**.
37. Gatan, I. P., *CA Digital Micrograph 1.71.38*, 2010.
38. Kilaas, R. *MacTempas Software, version 2.3.7; Total Resolution Inc.: Berkeley, CA*, 1988.
39. Alonso, J. A.; Martinez-Lope, M. J.; de la Calle, C.; Pomjakushin, V., Preparation and structural study from neutron diffraction data of RCoO₃ (R = Pr, Tb, Dy, Ho, Er, Tm, Yb, Lu) perovskites. *Journal of Materials Chemistry* **2006**, 16, (16), 1555-1560.

40. Shannon, R. D., Revised Effective Ionic Radii and Systematic Studies of Interatomic Distances in Halides and Chalcogenides. *Acta Crystallographica A* **1976**, 32, 751.
41. Radaelli, P. G.; Cheong, S. W., Structural phenomena associated with the spin-state transition in LaCoO_3 . *Phys. Rev. B* **2002**, 66, (9), 094408.
42. Sahu, S. K.; Tanasescu, S.; Scherrer, B.; Marinescu, C.; Navrotsky, A., Energetics of lanthanide cobalt perovskites: LnCoO_{3-d} (Ln = La, Nd, Sm, Gd). *Journal of Materials Chemistry A* **2015**, 3, (38), 19490-19496.
43. Giblin, S. R. PhD Thesis. University of Durham, Durham, 2006.

Graphical Abstract



The series of perovskite rare-earth (RE) doped cobaltites (RE)CoO₃ (RE = La – Dy) was prepared by microwave-assisted synthesis. The well-known magnetism in LaCoO₃, which involves a thermally induced Co³⁺ (d⁶) low spin to intermediate or high spin state transition, is strongly modified by RE-doping and a rich variety of magnetic order has been detected across the series.